13th ewtec 2019 Proceedings of the 13th European Wave and Tidal Energy Conference 1-6 Sept 2019, Naples, Italy

CCP-WSI Blind Test Series 2: Assessment of focused wave impacts on floating WECs using OpenFOAM

Scott A. Brown, Edward J. Ransley, and Deborah M. Greaves

***Abstract*—The presented work represents an individual contribution to the CCP-WSI Blind Test Series 2, in which the submitted results are compared against both physical and alternative numerical solutions for varying wave steepness achieved through changes in peak frequency. Reducing the time taken to provide reliable results is critical if computational fluid dynamics (CFD) is to become a routine design tool for offshore renewable energy devices. This can potentially be achieved by simplifying simulation setup, and hence reducing the required man-hours, through standardised 'best practice' procedures. Therefore, in the absence of validation data, the scope of this study is to provide a 'blind' estimation of numerical accuracy in simulations of focused wave interactions with floating wave energy converters (WECs). The present numerical results are obtained using open-source CFD with waves generated via linear superposition of first order wave components, derived from empty tank data. Two geometries are considered and the effect of wave steepness on surge, heave and pitch motion, along with the load in the mooring, is examined. Based solely on the reproduction of the known empty tank data, the numerical predicitons are estimated to be within 10% of the experimental data in peak motion and mooring loads.**

***Index Terms*—Error Estimation, Wave Energy, CFD, Extreme Events, NewWave, uncertainty**

I. Introduction

UNCERTAINTY in the accuracy of numerical solutions is one of the key issues that is limiting the use of computational fluid dynamics (CFD) as a routine design tool, along with the time taken to obtain reliable results. The time taken to run a simulation is notoriously large, but this can be decreased through use of a larger computational resource, which is becoming increasingly available. However, an often-overlooked factor is the number of man-hours required to setup a case through processes such as mesh design [1], which, from experience, is potentially larger than the simulation time. For industry to benefit from the high volume of information that CFD models can provide, the setup process must be streamlined, and one way that this could be achieved is through parametric understanding of numerical accuracy and providing standardised, 'best practice' procedures.

This paper (#1294) has been submitted to the Wave hydrodynamic modelling track at EWTEC2019. This work was supported in part by the EPSRC funded CCP-WSI project (EP/M022382/1) and represents the authors contribution to the CCP-WSI Blind Test Series 2.

S. Brown, E. Ransley and D. Greaves are with the School of Engineering, University of Plymouth, Drake Circus, Plymouth, UK, PL48AA (e-mail: scott.brown@plymouth.ac.uk; edward.ransley@plymouth.ac.uk; deborah.greaves@plymouth.ac.uk).

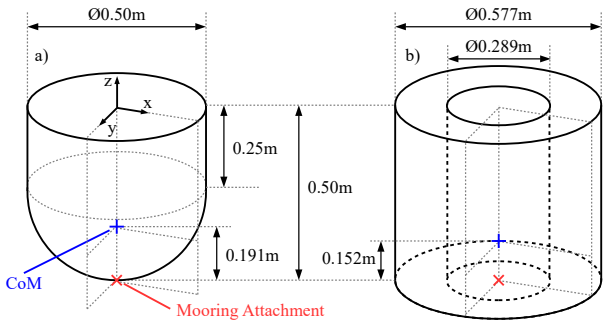

Fig. 1. The two geometries from CCP-WSI Blind Test Series 2: Geometry 1 (a) is a hemispherical-bottomed buoy; Geometry 2 (b) is a cylindrical structure with a moonpool.

Therefore, the scope of this work is to provide a 'blind' estimation of numerical accuracy, based purely on the reproduction of empty tank data. This approach was previously utilised for a case with a fixed structure, but here the focus is on the interaction of focused wave events with floating structures that represent a simplified wave energy converter (WEC). The presented work represents an individual contribution to the CCP-WSI Blind Test Series 2 [2], in which the submitted results are compared against both physical and alternative numerical solutions for varying peak wave frequency. The numerical results are obtained using the open-source C++ libraries of OpenFOAM (version 5.0) to solve the Reynolds-Averaged Navier-Stokes (RANS) equations. Wave generation is achieved via linear superposition of first order wave components, derived from the empty tank data, and the relaxation zone method from the waves2Foam toolbox [3] is used for absorption. Two different geometries are considered: a hemispherical-bottomed buoy; and a cylindrical structure with a moon-pool (Figure 1). For both structures, the effect of wave steepness on the surge, heave and pitch motion of the structure, along with the load in the mooring, caused by varying peak wave frequency, is examined.

II. CCP-WSI Blind Test 2 Case Studies

CCP-WSI Blind Test Series 2 concerns the response of floating surface-piercing structures, representing simplified WECs, to focused wave events varied in steepness through changes in peak frequency [2]. Two different structures are considered: Geometry 1 is a hemispherical bottomed buoy 0.5 m in diameter, 0.5 m in

TABLE I
GEOMETRIES CONSIDERED IN CCP-WSI BLIND TEST SERIES 2

ID	mass [kg]	$z_{com,rel}$ [m]	draft [m]	I_{xx} [kgm^2]	I_{zz} [kgm^2]
Geometry 1	43.674	0.191	0.322	1.620	1.143
Geometry 2	61.459	0.152	0.330	3.560	3.298

TABLE II
WAVE CONDITIONS USED IN CCP-WSI BLIND TEST SERIES 2

ID	ka [-]	h [m]	A_n [m]	f_p [Hz]	H_s [m]	L_c [m]
Wave 1	0.129	3.000	0.250	0.358	0.274	11.34
Wave 2	0.161	3.000	0.250	0.400	0.274	9.407
Wave 3	0.193	3.000	0.250	0.438	0.274	7.985

height (Figure 1a); Geometry 2 is also 0.5 m in height but is a 0.577 m diameter cylinder with a 0.289 m diameter moonpool (Figure 1b). Both geometries are moored using the same linear spring mooring with stiffness 67 N/m and a restlength of 2.199 m, attached at the centreline, and bottom of the structure ($\times$ in Figure 1). The geometries have similar draft but the remaining properties are substantially different (Table I). Geometry 2 has larger mass; lower centre of mass ($+$ in Figure 1); and larger moment of inertia. Three focused wave events are considered with varying steepness ranging from $ka = 0.129$ to $ka = 0.193$ (Table II). The steepness is changed by altering the peak frequency, f_p (and hence the characteristic wavelength L_c), whilst keeping the water depth ($h = 3$ m), amplitude ($A_n = 0.25$ m), and significant wave height ($H_s = 0.274$ m) constant (Table II).

III. NUMERICAL MODEL

This work utilises the open-source CFD software, OpenFOAM, which is based on the finite volume discretisation. The `interFoam` solver, modified for wave generation, is used to solve the two-phase, incompressible, Reynolds-Averaged Navier-Stokes (RANS) equations

$$\frac{\partial(\rho\mathbf{u})}{\partial t} + \nabla\cdot(\rho\mathbf{u}\mathbf{u}) = -\nabla p + \nabla^2(\mu\mathbf{u}) + \rho\mathbf{g}\nabla\cdot\mathbf{u} = 0, \quad (1)$$

where p is the pressure, $\mathbf{u} = (u, v, w)$ is the fluid velocity and $\mathbf{g}$ is acceleration due to gravity [4]. The fluid density, ρ, and dynamic viscosity, μ are determined using the volume of fluid (VOF) interface capturing scheme

$$\frac{\partial\alpha}{\partial t} + \nabla\cdot(\mathbf{u}\alpha) = 0, \rho = \rho_1\alpha + \rho_2(1-\alpha), \mu = \mu_1\alpha + \mu_2(1-\alpha), \quad (2)$$

where α is an indicator function representing the phase fraction of each mesh cell, and subscripts 1 and 2 represent air and water, respectively [4].

A. Wave Generation

The data supplied from the experimental campaign is surface elevation time series' at a finite number of spatial locations, obtained using wave gauges. Wave generation has been achieved using the waves2Foam toolbox [3], which allows the free surface and velocity profiles at the inlet boundary to be calculated using linear superposition of N wave components. For example, the free surface profile is calculated using

$$\eta = \sum_{i=1}^{N} a_i \cos(\omega_i t - k_i x + \phi_i), \quad (3)$$

where a_i, k_i, ω_i and ϕ_i are the amplitude, wavenumber, frequency and phase, respectively, of the i^{th} wave component.

In this work the number of wave components, and their frequency, amplitude and phase values, are selected using Fast Fourier Transform (FFT) analysis of the time series obtained from the wave gauge furthest upstream in the empty tank experimental data. The FFT is used to transform the time series into frequency space, providing the wave frequencies, along with the corresponding amplitudes and phases, required to reproduce the time series. To increase the computational efficiency of the model ([5], [6]), the number of components is selected based on a methodology developed by Musiedlak et al. [7]; Experimental noise is filtered out using a low pass Butterworth digital and analog filter [8], before the FFT is taken, and the resulting wave frequencies are sorted from largest to smallest amplitude. Each wave component is then systematically added to make a signal which is compared with the original time series. The number of components, N, is selected as the smallest possible quantity that achieves a user defined tolerance,. In previous work ([5], [6]), this user-defined tolerance was based solely on the cross-correlation coefficient of the experimental and numerical signals. In this study, the approach is extended to obtain the minimum value of N that satisfies the user-defined tolerance for multiple criteria: cross-correlation coefficient; maximum peak height; and maximum trough depth.

This methodology only guarantees that the signal will be within the specified tolerance at the inlet boundary, and not necessarily elsewhere in the numerical wave tank, but only requires a few seconds to determine. Furthermore, the use of linear superposition neglects higher harmonics and hence the approach is expected to become increasingly inaccurate for highly nonlinear waves (i.e. high wave steepnesses). Therefore, the number of components required to reproduce the experimental data is discussed in more detail later (Section IV-C) and empty tank simulations (Section IV-E) are used to determine the accuracy of the approach at the focused location.

B. Numerical Setup

The numerical model is setup to represent a section of physical experiments in the COAST laboratory's Ocean Basin at the University of Plymouth [2]. Following the experimental setup, the water depth is set to 3 m, the waves are generated using the approach described above and propagate in the positive x direction (Figure 2). A numerical domain of length 25 m

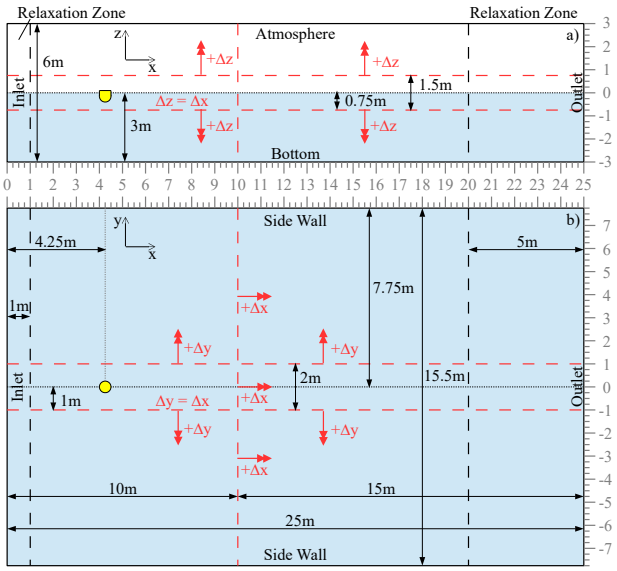

Fig. 2. Scale diagram of the numerical setup. Information in red denotes mesh properties with double headed arrows (↠) showing the direction of increasing mesh grading.

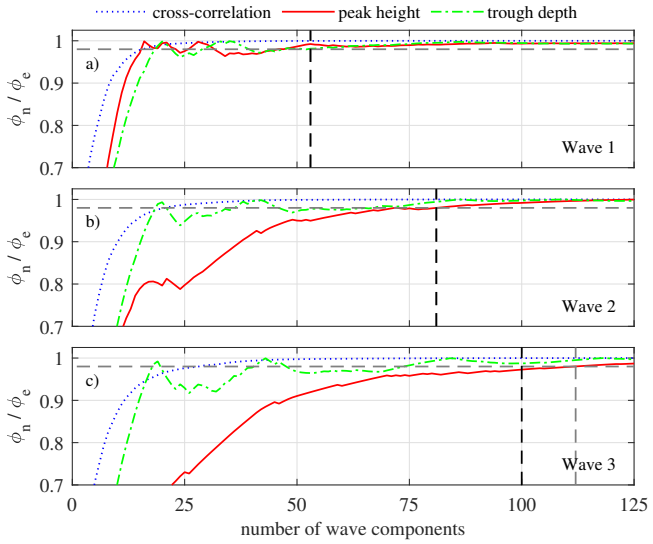

Fig. 3. Convergence of cross-correlation coefficient (· · · · ·), maximum peak height (——) and trough depth (– · –) as a function of N for Waves 1 (a), 2 (b) and 3 (c), along with the required N (– – –) to satisfy 2% tolerance, and the final N used (– – –).

$(0 \leq x \leq 25\,\text{m})$, width 15.5 m $(-7.75 \leq y \leq 7.75\,\text{m})$ and height 6 m $(-3 \leq z \leq 3\,\text{m})$ is used for all simulations, with the still water level located at $z = 0$ (Figure 2). The discretisation in the free surface region $(|z| \leq 0.75\,\text{m})$ is set to $\Delta z = 0.025\,\text{m}$ (Figure 2a), determined using a mesh convergence study as detailed later in the paper. A cell aspect ratio of 1 is used in the working region $(x \leq 10)$, in the vicinity of the platform $(y \leq 1\,\text{m})$ (Figure 2b). The centre of the model is positioned at $x = 4.25$ and $y = 0$, and is set to the draft observed at equilibrium in the experiments (Table I), with the mooring assumed to be anchored at (x,y,z) = (4.25,0,-3).

Following the results of CCP-WSI Blind Test Series 1 ([5], [6], [9]), it was found that reflections from side and end walls could be negatively influencing reproduction of focused wave events. Hence, in this work the length and width (set to the same as the COAST Ocean Basin) of the domain has been increased substantially to reduce these effects. Furthermore, the relaxation zone technique, included with the waves2Foam toolbox [3], is used to absorb wave reflections, with an inlet relaxation zone of 1 m and an outlet relaxation zone 5 m in length (Figure 2), which is approximately $0.5L_c$ or greater in all cases. The outlet relaxation zone is expected to produce a reflection coefficient of $0.1 - 0.3\%$ for all of the wave conditions considered in this work [3].

The necessity for such a large numerical domain makes the case computationally expensive, and hence mesh grading (indicated by double headed arrows, ↠, in Figure 2) is used to mitigate the cost by reducing the number of mesh cells: in the positive $x-$axis the mesh is constant discretisation $(\Delta x = 0.025\,\text{m})$ for $x \leq 10\,\text{m}$ before linearly increasing to $\Delta x = 0.5\,\text{m}$; in the y $(|y| > 1\,\text{m})$ and z $(|z| > 0.75\,\text{m})$ coordinates, the mesh increases to $\Delta y = \Delta z = 0.25\,\text{m}$ (Figure 2). The structures were meshed using `snappyHexMesh`: Geometry 1 does not require additional mesh refinement around the structure, but Geometry 2 requires two levels of octree refinement [10] to reproduce correctly. Once the structures are meshed, the mesh size is approximately 11 million cells in both cases.

IV. Blind Error

As mentioned previously, the work presented in this paper has been produced 'blind', i.e. without access to the experimental data with the structure in place, and if CFD is to become a robust design tool in the future, it is crucial that the error can be quantified using known parameters. In this work, the wave profile is the known parameter since physical empty tank data has been released, and this section aims to quantify and minimise discrepancies in the reproduction of the wave. This estimation will be assumed to relate to the motion of the geometries, and the validity of this assumption can be assessed in the future based on release of the full experimental data set at the end of CCP-WSI Blind Test Series 2.

C. Number of Wave Components

The first step in the reproduction of the wave is to determine an adequate number of wave components, N, to reproduce the signal at the inlet $(x = 0)$, whilst minimising computational cost. In previous work ([5], [6]), N was determined using a combination of the correlation between experimental and numerical signals and 2D simulations to analyse the solution at the focus location. The requirement to run a series of simulations to determine the inlet conditions is not practical, and here an approach that uses multiple criteria, and requires negligible time (relative to multiple calibration simulations), is utilised to obtain the minimum value of N: cross-correlation coefficient;

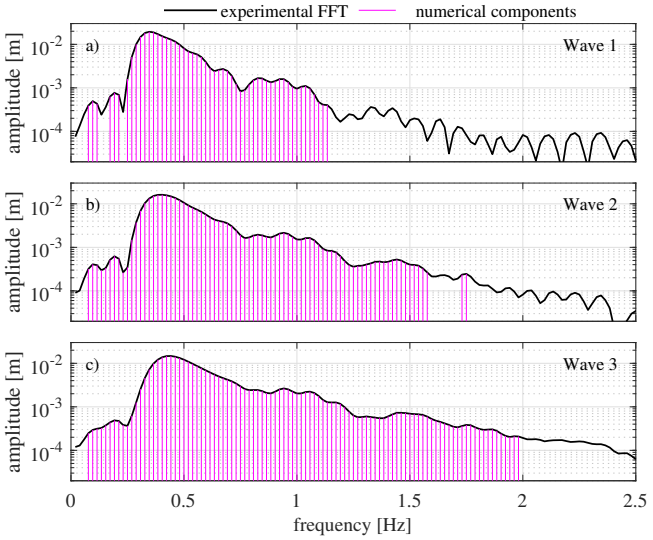

Fig. 4. Experimental amplitude spectrum (——) for Wave 1 (a), 2 (b) and 3 (c), and the selected components for the numerical model (——).

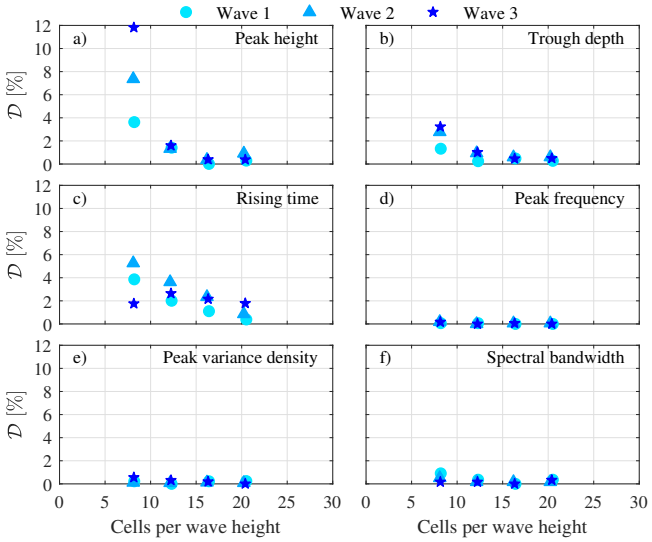

Fig. 5. Mesh convergence study for Wave 1 (●), Wave 2 (▲) and Wave 3 (★). The difference [%] in predictions of maximum peak height (a), maximum trough depth (b), rising time (c), peak frequency (d), peak variance density (e) and spectral bandwidth (f), on subsequent mesh resolutions.

maximum peak height; and maximum trough depth. An initial user-specified tolerance of 2% in each of the criterion is enforced, relative to the physical empty tank data, using the temporal range 35.3 to 50.3 s. However, previous experience has shown that instabilities can be introduced for large N (usually associated with steep waves), which are thought to be due to an inadequate capture of non-linear effects at the inlet boundary [6]. Therefore, a maximum value of $N = 100$ has been imposed. Figure 3 presents the convergence of the cross-correlation coefficient (· · · · · ·), maximum peak height (——) and maximum trough depth (— · —) for Wave 1 (a), Wave 2 (b) and Wave 3 (c) with N, along with the minimum N required for a 2% tolerance of all criteria (– – –), and the final value for N used in this work (– – –). The required value for N increases with wave steepness, with the cross-correlation coefficient generally converging fastest and the peak height slowest. For the steepest wave (Figure 3c), N exceeds the imposed threshold and hence 100 components is used for this wave. Consequently, there is likely to be some error in the numerical predictions of peak height in this case since it is only converged within 3%.

Figure 4 presents the FFT of the experimental data (——) and the individual frequency components used in the numerical model (——) for Wave 1 (a), Wave 2 (b) and Wave 3 (c). The peak frequency of the spectra can be seen to be increasing with steepness (as expected), and the selected components are generally in a block around the peak frequency. However, there are occasionally frequencies which are separated from the main block (e.g. the higher frequency components in Wave 2). It is possible that these components are artefacts of the experimental facility (e.g. reflections from the beach), that are being captured by the present component selection procedure. Therefore, in the future, the present methodology may require further refinement in order to correctly identify and discard components which are solely due to experimental procedures.

D. Mesh Resolution

A mesh convergence study is now conducted for each of the three focused waves, generated using the number of components selected in Section IV-C. To determine the required resolution, each of the waves are run on a series of 2D uniform meshes of increasing resolution, and the percentage difference between one mesh and the next coarsest is plotted in Figure 5 at the focus location ($x = 4.25$). In previous work ([5], [6]), the convergence of the mesh was determined using a single root mean square (RMS) parameter. In this work, multiple criteria, based on parameters which will be supplied to the CCP-WSI Blind Test Series 2, are used to determine the discretisation. These criteria are plotted in Figure 5 as a function of cells per wave height and are a combination of time and frequency domain parameters. The time domain variables are maximum peak height (a), maximum trough depth (b), and rising time (c); and the frequency criteria are peak frequency (d), peak variance density (e) and spectral bandwidth (f) [2]. The results imply that maximum trough depth and all frequency criteria converge to within 1% for relatively coarse mesh resolutions. However, the rising time and maximum peak height converge slower: the former parameter only achieves a 2% convergence in the steepest case due to asymmetry and higher order effects associated with being near the breaking limit (see Section IV-E), similar to previous work [11]. Overall, however, the results are reasonably good for all of the meshes and hence mesh resolution was chosen as the second finest ($\Delta x = 0.025$ m) since all parameters converged to approximately 2% or less at this resolution. This resolution is expected to perform well since it is considerably finer than that used by Ransley et al. ([12], [13]), who previously simulated the interaction of a similar focused wave event with a hemi-spherical buoy using a mesh discretisation of 0.037 m in the free surface region, showing good agreement.

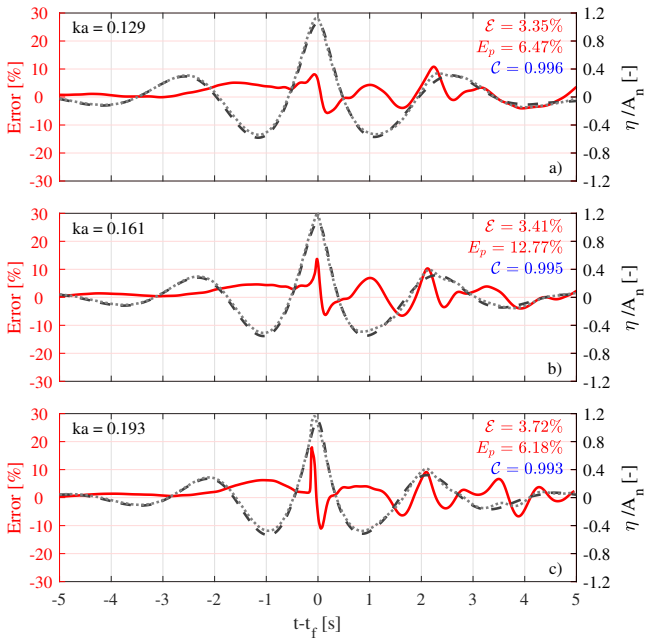

Fig. 6. Relative error (——) in the numerical (· · · · · ·) 3D empty tank free surface predictions relative to the experimental data (– – –). Also shown is the RMS error ($\mathcal{E}$), peak amplitude error (E_p) and cross-correlation coefficient ($\mathcal{C}$) of the experimental and numerical signals.

E. Error Time Series

Simulations are now run using the numerical setup described in Section III-B (which incorporates the conclusions of Sections IV-C and IV-D), without the structures in place, to determine the accuracy of the reproduction of the experimental empty tank data. Figure 6 presents the numerical (· · · · · ·) and experimental (– – –) surface elevation signals at the focus location, normalised by the amplitude, A_n, for Wave 1 (a), Wave 2 (b) and Wave 3 (c). Also shown (——) is the relative error [%] in the numerical solution, normalised by A_n, along with the RMS ($\mathcal{E}$), error in maximum amplitude (E_p) and cross-correlation coefficient ($\mathcal{C}$) of the two signals. The reproduction of Wave 1 is good ($< 10\%$, $\mathcal{E} \approx 3\%$) throughout, although the larger discrepancies occur after the focus event and are thought to be due to wave reflections in both the numerical and experimental data. Waves 2 and 3 are also largely acceptable ($< 10\%$) and have similar mean error ($\mathcal{E} \approx 3\%$) as Wave 1, but larger spikes can be observed around the main peak, $10-20\%$ in magnitude. In the steeper wave (Figure 6c), this is partially due to an asymmetry in the numerical data, leading to an over-prediction before the experimental event, and an under-prediction after. This shows that an amplitude based approach (such as the RMS) can be very sensitive to phase discrepancies and although in this case the majority of the signal is in phase with the experimental data ($\mathcal{C} > 0.99$), a more reliable indicator may be required for future work. Considering just the error in the amplitude of the main peak height (E_p), all three cases are overestimated with largest error in Wave 2 ($E_p = 12.77\%$), and substantially less in the other cases ($E_p \approx 6\%$). Having larger peak amplitude error for the middle steepness is slightly surprising but is likely due to premature breaking in the numerical model reducing the wave height in Wave 3, which is consistent with the asymmetric profile in this case. Although the error in peak magnitude is reduced, the overall error in the steepest case will most likely be higher (as seen in the value of $\mathcal{E}$) and this highlights the need for multiple

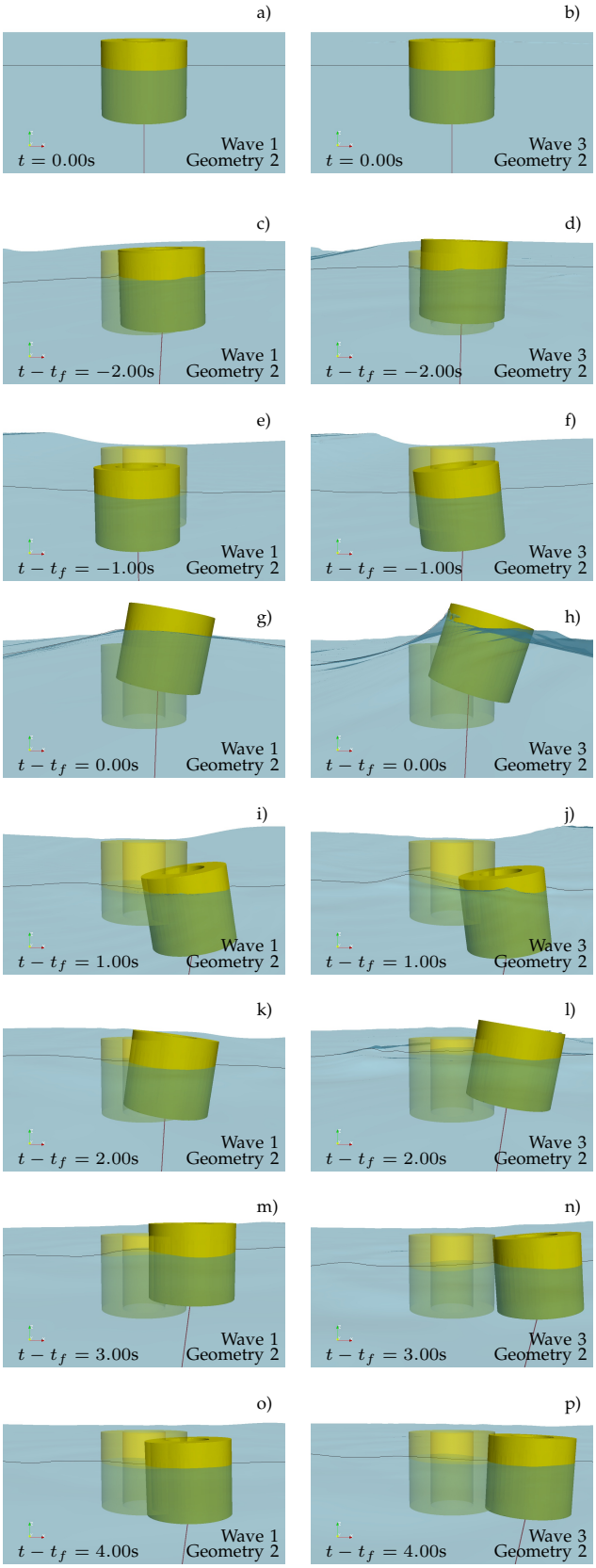

Fig. 7. Snapshots of Geometry 2 in Waves 1 (left) and 3 (right) at various times. The mooring (red) and initial position of the device (transparent yellow) are included for reference.

criteria when assessing such problems.

Based on previous experience ([11], [12]), it is thought that the error in heave response will be similar to the reproduction of the wave ($\approx 10\%$). Conversely, the surge and pitch responses may be functions of additional parameters such as wave velocity, wave phase and drag, making it harder to estimate error in these cases but are also thought to be approximately 10% [12]. However, the coupled nature of the problem, and the presence of the mooring, could lead to much larger discrepancies.

V. Blind Results

Results are now presented when each of the structures is in place. Since experimental data is not available the trends in the numerical results are discussed and are split into two sections: the effect of wave steepness on the motion of a device; and secondly the differences between the two geometries considered here.

F. Effect of Wave Steepness

Figure 7 presents numerical snapshots of the position of Geometry 2 in Waves 1 (left) and 3 (right) at similar times relative to the focus time, t_f, along with the position of the device at $t = 0.00\,\mathrm{s}$ and mooring line (red). Qualitatively, the snapshots imply that the surge and pitch motions of the device increase with wave steepness, whereas the heave is less affected. It is also apparent that Wave 3 is breaking at time $t - t_f = 0.00\,\mathrm{s}$. The present mesh is not designed to resolve the breaking process accurately since this would be excessively computationally expensive, and the simulation is not being run using a turbulence model since the flow is expected to be largely laminar. Therefore, it is likely that this is contributing to the discrepancies in peak magnitude and the asymmetry observed in Figure 6c.

Figure 8 presents a more quantitative comparison of the numerical results in the form of time series (5 seconds either side of the focus time, t_f) for $ka = 0.129$ (– · –), $ka = 0.161$ (——) and $ka = 0.193$ (– – –). The empty tank surface elevation signal (a,b), surge (c,d), heave (e,f), pitch (g,h) and total mooring load (i,j) are presented for Geometry 1 on the left (a,c,e,g,i) and Geometry 2 on the right (b,d,f,h,j). The empty tank data (Figure 8a,b) shows the anticipated trends in surface elevation: the peak heights are similar for all three waves but the rising time decreases with increasing steepness, due to the increase in peak frequency. The heave peak magnitudes are similar for all three waves, but the phase is altered similar to the surface elevation. This implies that the heave response is strongly correlated ($\mathcal{C} > 0.85$) with the surface elevation, as hypothesised in Section IV-E. Defining normalised maximum responses as the magnitude of the first peak occurring at or after the focus event, normalised by peak magnitude of the empty tank wave prediction, the heave response ($0.8 - 0.86\,\mathrm{m/m}$), is seen to remain reasonably constant with wave height (Table III) for Geometry 1. Although this indicates that heave is a linear relationship with wave amplitude, the

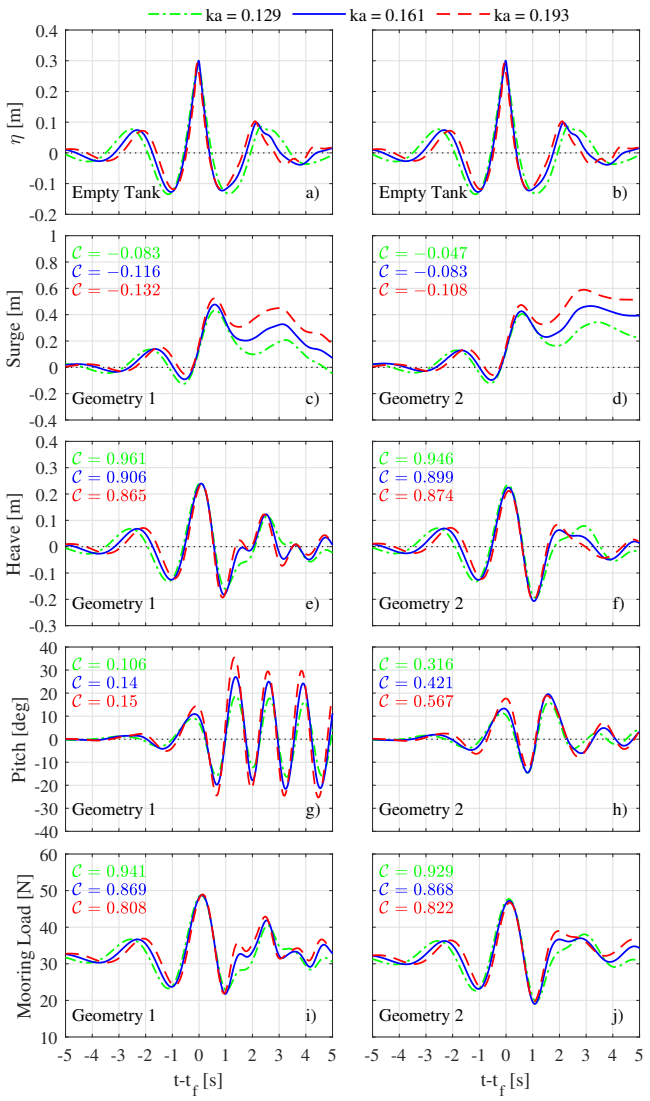

Fig. 8. Numerical predictions for $ka = 0.129$ (– · –), $ka = 0.161$ (——) and $ka = 0.193$ (– – –). The empty tank surface elevation signal (a,b), surge (c,d), heave (e,f), pitch (g,h) and total mooring load (i,j) are presented for Geometry 1 on the left (a,c,e,g,i) and Geometry 2 on the right (b,d,f,h,j). The cross-correlation coefficient ($\mathcal{C}$) of each parameter and the empty tank surface elevation data is indicated in the corresponding colour.

normalised response of Geometry 2 reduces slightly with wave steepness (consistent with previous work [11]), implying that other factors based on geometry may need to be considered when estimating error in heave. The relationship between heave and surface elevation magnitude may be complicated here by the wave breaking observed in Wave 3, and suggests that a larger sample of wave conditions and geometries is required in order to fully understand the problem. Hence, for simplicity, in this work it is assumed that the reproduction of the empty tank amplitude will be a reasonable indicator in heave error for both geometries: the over-estimation in empty tank peak surface elevation are predicted to lead to $4.5 - 10\%$ over-prediction in peak heave.

Unlike the heave response, the surge and pitch motions do not correlate with the surface elevation ($|\mathcal{C}| < 0.3$), implying that the behaviour in these degrees of freedom does not depend solely on the

TABLE III
NORMALISED MAXIMUM RESPONSE IN INTERVAL $|t - t_f| \leq 1$

Geometry	1	1	1	2	2	2
Wave	1	2	3	1	2	3
Surge [m/m]	1.53	1.59	1.80	1.44	1.42	1.63
Heave [m/m]	0.86	0.80	0.82	0.83	0.75	0.73
Pitch [deg/m]	32.1	36.3	49.7	39.8	44.3	60.7

amplitude. Although the signals are not in phase with the surface elevation, wave steepness does play a role since both pitch and surge increase in peak magnitude, which can also be observed in the normalised maximum responses in these parameters (Table III). Consequently, these parameters are harder to relate to solely the wave amplitude and it is thought that other factors, such as the phase of the wave, drag, flow velocity or mooring load could play a larger role in these degrees of freedom. This conclusion is consistent with the analysis of Figure 7, which implied that surge and pitch increase with steepness at a greater rate than heave. Based on previous experience with similar structures [13], the predictions of maximum surge and pitch are good if the wave amplitude is captured well, but the secondary peaks are usually under-estimated. Hence, it is estimated that the error in the maximum surge and pitch will be less than 10%, with potential to be much greater (up to 50%) after the focus event.

The mooring load (Figures 8i,j) is strongly correlated with both the surface elevation and heave response (Figures 8e,f), due to the small horizontal offsets relative to the vertical, which includes the water depth. Hence, it is anticipated that the mooring load will be over-estimated by a similar margin as the heave.

G. Effect of Geometry

As well as showing the consequences of increasing wave steepness, Figure 8 shows interesting differences between the motion of the two geometries. The most noticeable difference is in the pitch motion (Figure 8g,h) of the two geometries: both have similar behaviour before $t = t_f$, but after the focus event, Geometry 1 has large pitch motion (up to 40°) and continues to oscillate, whereas Geometry 2 pitches substantially less and the motion has substantially higher damping. This damping is thought to be primarily due to piston and sloshing effects generated by the moonpool ([14], [15]), although it should be noted that the different mass properties and geometry of the device (e.g. differences in metacentric height) are also likely to be a factor. In the future, it may be interesting to isolate and quantify the effect of the moonpool numerically by considering a solid cylinder with the same mass properties as Geometry 2. Considering the other degrees of freedom, the magnitude of the surge motion (Figure 8c,d) is comparable, and the numerical model predicts that three peaks will occur for both geometries (in the range of times shown). However, Geometry 1 has maximum surge in the second peak whereas Geometry 2 surges furthest in the third peak. This could potentially be related to the reduced pitching motion of Geometry 2, which may be leading to increased drag on the device, or be caused by additional momentum caused by the larger mass of the device. The phases of the heave and surge motions are similar for both devices: the maximum heave occurs immediately after

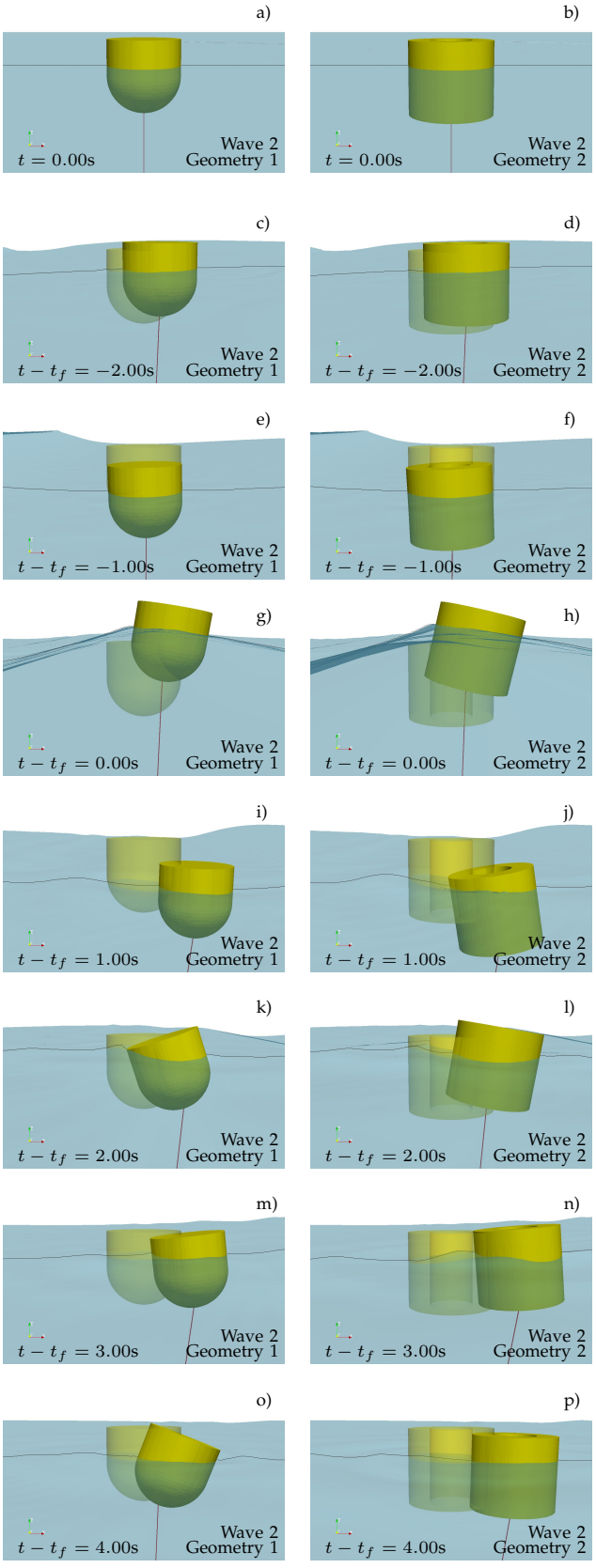

Fig. 9. Snapshot comparison of the two geometries at various phases of Wave 2. The mooring (red) and initial position of the device (transparent yellow) are shown for reference.

TABLE IV
REQUIRED COMPUTATIONAL EFFORT FOR EACH CASE

Geometry		1	1	1	2	2	2
Wave		1	2	3	1	2	3
# Cells	[-]	11M	11M	11M	11M	11M	11M
Clock Time	[hrs]	31.1	42.1	52.8	43.3	60.5	78.5
CPUs	[-]	128	128	128	128	128	128
Exec. Time	[cpu hrs]	3984	5385	6754	5543	7740	10053
Max Co.	[-]	0.5	0.5	0.5	0.5	0.5	0.5
max δt	[ms]	8.8	13	14	5.6	6.0	5.8
min δt	[ms]	0.3	0.3	0.2	0.1	0.2	0.1
mean δt	[ms]	1.4	1.4	1.4	1.0	0.9	0.9

the focus event, surge is slightly delayed (maximums occur ≈ 0.5 s after the wave). Figure 9 presents numerical visualisations of Geometries 1 (left) and 2 (right) at times $t = 0.00$ s (a,b); $t - t_f =$ -2.00 s (c,d); -1.00 s (e,f); 0.00 s (g,h); 1.00 s (i,j); 2.00 s (k,l); 3.00 s (m,n); and 4.00 s (o,p). As was observed in Figure 8, the motion of the two devices is similar up until $t - t_f = 0.75$ s, but after this time the pitch motion of Geometry 2 is damped whereas Geometry 1 continues to pitch substantially. Furthermore, Geometry 2 has relatively large positive surge for longer than Geometry 1, which can be observed to return close to the equilibrium surge position within 5 s of the focus event.

H. Hardware and Execution Time

The simulations detailed in the above analysis were run using the in-house high performance computing service at the University of Plymouth. This facility consists of 52 2U Twin Sq. (4 Nodes) networked with Intel Omni-Path cabling, and equipped with dual Intel E5-2683v4 8 core 2.5 GHz processors with 128 GB of memory per motherboard. Each simulation was run using 128 processors (≈ 86000 cells per processor) and the computational effort required for each case is presented in Table IV. The required clock times range from $30 - 80$ hours ($\sim 4000 - 10000$ CPU hrs), and show an increase with wave steepness, which is a consequence of higher non-linearity and increased wave components ([5], [6]). Furthermore, simulations of Geometry 2 are substantially more expensive, which is thought to be a combination of increased mesh resolution on the device, and the modelling of the moonpool region. Although the present approach could potentially be made more computationally efficient by using symmetry planes or through thorough scaling tests [11], it is expected to be substantially larger relative to other, lower-fidelity models (such as those based on potential wave theory) that are providing contributions to the CCP-WSI Blind Test Series 2. However, it is anticipated that the reproduction of the device's motion will be captured more accurately by the present model than the lower-fidelity approaches, particularly as the non-linearity of the wave increases, but the extent will not be known until the final results of the CCP-WSI Blind Test Series 2 are released.

VI. CONCLUSION

Numerical simulations of focused wave interactions with simplified floating WECs using the open source CFD software, OpenFOAM, have been presented as part of a contribution to the CCP-WSI Blind Test Series 2. The effect of peak-frequency altered wave steepness is investigated, and a 'blind' estimate of the error in the present model is provided, based solely only on reproduction of released empty tank data [2]. The empty tank reproduction was generally good (RMS error $\mathcal{E} \approx 3\%$) although the peak magnitude was consistently over-estimated ($E_p = 6 - 12\%$). Since the peak heave response and mooring loads strongly correlate ($\mathcal{C} > 0.8$) with the surface elevation signal, the focused event the 'blind' error was estimated as $4.5 - 10\%$. The error in peak surge/pitch varied non-linearly with wave amplitude which reduces confidence in error estimations based on surface elevation, but is estimated as $\approx 10\%$ based on previous experience. Future effort should aim to verify the 'blind' error estimations presented here following the release of the full CCP-WSI Blind Test 2 dataset.

ACKNOWLEDGEMENT

The physical data presented here was generated as part of the EPSRC funded CCP-WSI project (EP/M022382/1) and is distributed, along with the numerical solutions, via the CCP-WSI project website (http://www.ccp-wsi.ac.uk/).

REFERENCES

[1] P. Schmitt, K. Doherty, D. Clabby, and T. Whittaker, "The opportunities and limitations of using CFD in the development of wave energy converters," in *International Conference on Marine and Offshore Renewable Energy*, London, UK, 2012, pp. 1–9.

[2] CCP-WSI. (2019) Focused wave interactions with floating structures (CCP-WSI Blind Test Series 2). [Online]. Available: https://www.ccp-wsi.ac.uk/blind_test_series_2

[3] N. G. Jacobsen, D. R. Fuhrman, and J. Fredsøe, "A wave generation toolbox for the open-source CFD library: OpenFOAM®," *International Journal for Numerical Methods in Fluids*, vol. 70, pp. 1073–1088, 2012.

[4] H. Rusche, "Computational fluid dynamics of dispersed two-phase flows at high phase fractions," Ph.D. dissertation, Imperial College of Science, Technology & Medicine, 2002.

[5] S. Brown, P.-H. Musiedlak, E. Ransley, and D. Greaves, "Numerical simulation of focused wave interactions with a fixed FPSO using OpenFOAM 4.1," in *Proceedings of the 28th International Ocean and Polar Engineering Conference*, Sapporo, Japan, 2018, pp. 1–6.

[6] ——, "Quantifying the predictive capability of OpenFOAM 4.1: Focused wave interactions with a fixed FPSO," *International Journal of Offshore and Polar Engineering*, vol. In Press, 2019.

[7] P.-H. Musiedlak, E. Ransley, D. Greaves, B. Child, M. Hann, and G. Iglesias, "Investigations of model validity for numerical survivability testing of WECs," in *Proceedings of the 12$^{\text{th}}$ European Wave and Tidal Energy Conference (EWTEC)*, Cork, Ireland, 2017, p. 8.

[8] S. Butterworth, "On the theory of filter amplifiers." *Experimental Wireless & the Wireless Engineer*, vol. 7, pp. 536–541, 1930.

[9] E. Ransley, S. Yan, S. Brown, D. Mai, T. Graham, Q. Ma, P.-H. Musiedlak, A. Engsig-Karup, C. Eskilsson, Q. Li, J. Wang, Z. Xie, V. Sriram, T. Stoesser, Y. Zhuang, Q. Li, D. Wan, G. Chen, H. Chen, L. Qian, Z. Ma, C. Mingham, D. Causon, I. Gatin, H. Jasak, V. Vukčević, S. Downie, P. Higuera, E. Buldakov, D. Stagonas, Q. Chen, J. Zang, and D. Greaves, "A blind comparative study of focused wave interactions with a fixed FPSO-like structure (CCP-WSI Blind Test Series 1)," *International Journal of Offshore and Polar Engineering*, vol. In Press, 2019.

[10] D. M. Greaves, "A quadtree adaptive method for simulating fluid flows with moving interfaces," *Journal of Computational Physics*, vol. 194, pp. 35–56, 2004.

[11] S. Brown, P.-H. Musiedlak, E. Ransley, and D. Greaves, "Numerical investigation of focused wave impacts on floating wave energy converters using OpenFOAM," in *Proceedings of the 29th International Ocean and Polar Engineering Conference*, Hawaii, USA, 2019, pp. 1–8.
[12] E. Ransley, "Survivability of wave energy converter and mooring coupled system using CFD," Ph.D. dissertation, Plymouth University, 2015.
[13] E. Ransley, D. Greaves, A. Raby, D. Simmonds, M. Jakobsen, and M. Kramer, "RANS-VOF modelling of the wavestar point absorber," *Renewable Energy*, vol. 109, pp. 49–65, 2017.
[14] B. Molin, "On the piston and sloshing modes in moonpools," *Journal of Fluid Mechanics*, vol. 430, pp. 27–50, 2001.
[15] O. M. Faltinsen, O. F. Rognebakke, and A. N. Timokha, "Two-dimensional resonant piston-like sloshing in a moonpool," *Journal of Fluid Mechanics*, vol. 575, pp. 359–397, 2007.